SAGE-Hindawi Access to Research
Enzyme Research
Volume 2011, Article ID 642758, 11 pages
doi:10.4061/2011/642758

Research Article

Enzyme Mechanism and Slow-Onset Inhibition of *Plasmodium falciparum* Enoyl-Acyl Carrier Protein Reductase by an Inorganic Complex

Patrícia Soares de Maria de Medeiros,[1] Rodrigo Gay Ducati,[2] Luiz Augusto Basso,[2] Diógenes Santiago Santos,[2] and Luiz Hildebrando Pereira da Silva[1]

[1] *Instituto de Pesquisas em Patologias Tropicais (IPEPATRO), Rua da Beira 7671, Rodovia BR364 km 3.5, 76812-245 Porto Velho, RO, Brazil*
[2] *Centro de Pesquisas em Biologia Molecular e Funcional (CPBMF), Pontifícia Universidade Católica do Rio Grande do Sul (PUCRS), Avenida Ipiranga 6681/92-A, 90619-900 Porto Alegre, RS, Brazil*

Correspondence should be addressed to Luiz Augusto Basso, luiz.basso@pucrs.br and Luiz Hildebrando Pereira da Silva, hildebrando.pereira@yahoo.com.br

Received 22 December 2010; Accepted 25 January 2011

Academic Editor: Qi-Zhuang Ye

Malaria continues to be a major cause of children's morbidity and mortality worldwide, causing nearly one million deaths annually. The human malaria parasite, *Plasmodium falciparum*, synthesizes fatty acids employing the Type II fatty acid biosynthesis system (FAS II), unlike humans that rely on the Type I (FAS I) pathway. The FAS II system elongates acyl fatty acid precursors of the cell membrane in *Plasmodium*. Enoyl reductase (ENR) enzyme is a member of the FAS II system. Here we present steady-state kinetics, pre-steady-state kinetics, and equilibrium fluorescence spectroscopy data that allowed proposal of *P. falciparum* ENR (PfENR) enzyme mechanism. Moreover, building on previous results, the present study also evaluates the PfENR inhibition by the pentacyano(isoniazid)ferrateII compound. This inorganic complex represents a new class of lead compounds for the development of antimalarial agents focused on the inhibition of PfENR.

1. Introduction

Malaria, a disease caused by a protozoan pathogen of the genus *Plasmodium*, remains one of the most devastating human diseases, causing as many as 250 million new cases and nearly one million deaths annually worldwide. This disease is especially worrisome in Africa, where one out of every five infant deaths is related to its effects [1]. Although malaria can be caused by mainly four species of the genus, *Plasmodium falciparum* is responsible for the most severe and deadly form of the disease and is to blame for 90% of malaria-related deaths occurring in African children below the age of five [2]. At present, the available drugs used to fight the disease are (a) aryl aminoalcohol compounds, such as quinine [3], (b) antifolates-dihydrofolate reductase inhibitors, such as pyrimethamine [4, 5], or (c) artemisinin derivatives [6]. Therapeutic treatment has, however, encountered serious obstacles, as this parasite has developed at least partial resistance to nearly every antimalarial regimen introduced to date, including the first-line drugs chloroquine and sulfadoxine-pyrimethamine [7]. As single-drug treatments are no longer adequate, combinations of two or more drugs will probably offer improved efficacy and reduced risk of emergence of drug-resistant parasites. Current examples of drug combinations are artemisinin-amodiaquine and artemether-lumefantrine (Coartem) [8]. The lack of an effective prophylactic vaccine and the generation and dissemination of drug-resistant strains clearly indicate the need for the development of new therapeutic approaches and identification of novel targets.

P. falciparum, a malarial parasite of the phylum Apicomplexa, has been found to contain an apicoplast, an organelle that originally arose from a cyanobacterium through a secondary endosymbiotic process, and, thus, possesses four membranes. During these endosymbiotic processes, resultant of millions of years of adaptive selection, the endosymbiont and host were integrated in a relationship involving gene losses and gene transfers, resulting in a reduction of the apicoplast genome to a bare minimum [9]. The majority of the apicoplast proteins are encoded by genes in the nuclear genome of the host, and the proteins that reside in the apicoplast and are encoded by the nucleus are posttranslationally targeted to the apicoplast organelle *via* the secretory pathway, owing to the existence of a bipartite N-terminal leader sequence [10]. In fact, the apicoplast is indispensable for the malarial parasite, since several vital metabolic processes for the parasite occur in this organelle. Among these processes are isoprene, haem, and fatty acid biosynthesis [11]. Fatty acid biosynthesis is critical for the parasite development as fatty acids are the major components of cell membranes. Moreover, fatty acids are important source of energy, play a key role in signal transduction as well as in protein acylation, and are needed for the growth, differentiation, and homeostasis in *P. falciparum*. It is also known that lipid biosynthesis is highly increased during the erythrocytic phases, when the parasite grows and divides extremely fast [12]. As the parasite invades its host, it attempts to protect itself by creating a so-called parasitophorous vacuole, in part as a protection from the host's immune system [13]. In this process, the parasite needs to produce its own fatty acids *de novo* so as to form and expand its membrane [14].

The enzymes involved in the biosynthesis of fatty acids are organized in two distinct ways within living systems. Fungi, mammals, and some mycobacteria accomplish fatty acid synthesis through the action of multifunctional proteins, each reaction being catalysed by a distinct region (domain) of these single-polypeptide proteins. These enzymes are classified as Type I fatty acid synthases (FAS I) and are also described as the "associative" type of fatty acid synthases, as successive steps in the fatty acid synthetic reaction occur at specific domains [15, 16]. In contrast, plants and many bacteria use the Type II or "dissociated" fatty acid synthases (FAS II), whose enzymes are best characterized in *Escherichia coli* [17]. Each step of the FAS II system is catalysed by a specific enzyme encoded by a separate gene. Since the FAS II is absent in humans, it represents a great opportunity for therapeutic applications. The fatty acid chain elongation module of FAS II consists of the cycling of the growing fatty acyl moiety through four key enzymes. Elongation is initiated by β-ketoacyl-ACP synthase I/II (FabB/FabF) enzyme, which catalyses the condensation of the growing fatty acyl ACP with malonyl-ACP to yield a β-ketoacyl-ACP with an additional two-carbon unit. The second step is the reduction of β-ketoacyl-ACP to β-hydroxyacyl-ACP catalysed by the β-ketoacyl-ACP reductase (FabG) enzyme. Water is then removed by β-hydroxydecanoyl-ACP dehydratase/isomerase (FabA) and/or β-hydroxyacyl-ACP dehydratase (FabZ) to produce 2-*trans*-enoyl-ACP. The final step in the elongation process is the NADH-dependent reduction of the double bond to produce fatty acyl ACP, which is catalysed by FabI, the only enoyl-ACP reductase (ENR) enzyme in *Plasmodium* (Figure 1). Successive elongation cycles typically lead to the formation of decanoic (C-10), lauric (C-12), and myristic (C-14) acids as the major fatty acyl ACPs in *Plasmodium* [13], whereas palmitic (C-16) acid is the most predominant fatty acid synthesized in humans [12].

ENR from *Mycobacterium tuberculosis* (MtInhA) was first identified as being the primary target for isoniazid (INH; Figure 2(a)) [18], the most prescribed drug to treat active tuberculosis. The enzyme is an NADH-dependent enoyl-ACP reductase specific for long-chain enoyl thioester substrates. MtInhA is a member of the mycobacterial FAS II, which elongates acyl fatty acid precursors of mycolic acids. INH is a prodrug that is activated by the de mycobacterial *katG*-encoded catalase-peroxidase enzyme in the presence of manganese ions, NAD (H) and oxygen [19, 20]. Approximately 50% of *M. tuberculosis* INH-resistant clinical isolates harbor deletions of, or missense mutations in, the *katG* gene [21, 22]. The KatG-produced acytylpyridine fragment of INH is covalently attached to the C4 position of NADH and forms a binary complex with the wild-type MtInhA [23]. This isonicotinoyl-NAD^+ adduct has been characterized spectroscopically and shown to bind to the enzyme with a dissociation constant value lower than 0.4 nM [24]. The isonicotinoyl-NAD^+ adduct has been shown to be a slow, tight-binding competitive inhibitor of wild-type MtInhA [25]. The initial rapidly reversible weak binding ($K_i = 16$ nM) is followed by a slow isomerization, leading to a tighter enzyme-inhibitor complex with an overall dissociation constant (K_i^*) value of 0.75 nM.

The mechanism of action of INH requires its conversion, by the mycobacterial KatG, into a number of electrophilic intermediates [20]. The formation of the adduct has been proposed to be formed through the addition of either an isonicotinic acyl anion to NAD^+ or an isonicotinic acyl radical to an NAD free radical [23]. The peroxidase activity of KatG catalyses the conversion of Mn^{2+} to Mn^{3+} [26]. Rapid freeze-quench electron paramagnetic resonance spectroscopy experiments have shown that hydrogen atom abstractions may be initiated by a KatG tyrosil radical [27]. Furthermore, it has been shown that the yield of isonicotinoyl-NAD^+ adduct is about the same after oxidation of INH by KatG or Mn^{3+} [28]. Accordingly, oxidation by Mn^{3+}-pyrophosphate has been proposed as an alternative method for nonenzymatic INH activation for simple chemical synthesis of various INH derivatives that mimic the isonicotinoyl-NAD^+ adduct [29]. Based on the activation mechanism proposed for INH, *via* an electron transfer reaction, an alternative self-activation inner-sphere electron transfer reaction route was proposed for designing new drugs for the treatment of INH-resistant and INH-sensitive tuberculosis. These drugs would be activated by electron transfer reactions before interacting with their cellular targets, and a redox reversible metal complex coordinated to the prodrug was employed as a prototype. Accordingly, we have recently demonstrated that pentacyano(isoniazid)ferrateII or

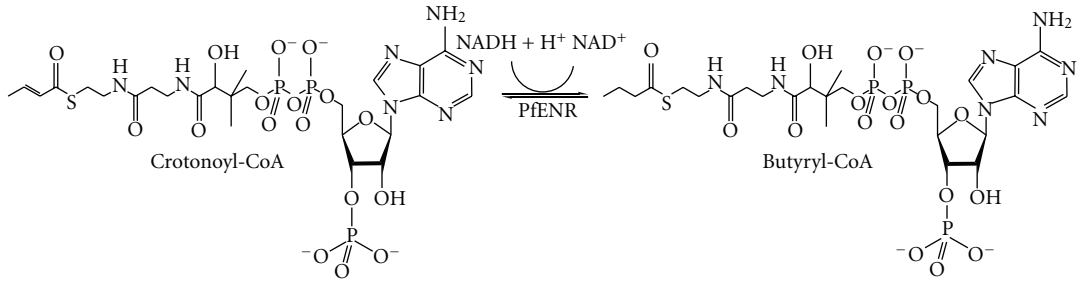

Figure 1: Reaction catalysed by PfENR.

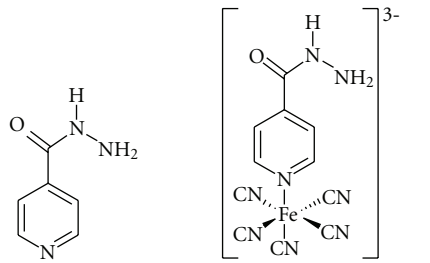

Figure 2: Chemical structure of isoniazid (a) and pentacyano(isoniazid)ferrateII (b).

$[Fe^{II}(CN)_5(INH)]^{3-}$ (Figure 2(b)) inhibits the activity of both wild-type and I21V mutant (INH-resistant) MtInhA enzymes [30]. The *in vitro* kinetics of inactivation indicates that this process requires no activation by KatG, no need for the presence of NADH, and is also effective against INH-resistant InhA mutants. An MIC value of $0.2\,\mu g\,mL^{-1}$ for this inorganic complex was determined by the radiometric BACTEC AFB system for the *M. tuberculosis* H37Rv strain, and toxicity assays in HL60 leukemia and MCS-7 breast cancer cells yielded an IC_{50} value greater than $25\,\mu g\,mL^{-1}$, thereby indicating a good selectivity index (SI = IC_{50}/MIC > 125; the Tuberculosis Antimicrobial Acquisition and Coordinating Facility of USA suggests that in order to a compound move forward through screening programs, SI should be larger than 10). More recently, we have shown that the $[Fe^{II}(CN)_5(INH)]^{3-}$ complex is a slow-onset inhibitor of MtInhA enzyme activity, with a true overall dissociation constant value of 70 nM [31]. In this mechanism of action an initial enzyme-inhibitor complex is rapidly formed, which then undergoes a slow isomerization reaction of an enzyme-inhibitor binary complex, where the inhibitor is more tightly bound to enzymes. The weakness in the use of classical enzyme inhibitors as drugs for clinical conditions is that inhibition results in the upstream accumulation of the substrate for the enzyme, which may overcome the inhibition. By contrast, the build-up of substrate cannot have any effect on the isomerization of the enzyme-inhibitor complex typical of the slow-onset mechanism and hence reversal of the inhibition [32].

The structural similarity between MtInhA and PfENR stimulated us to test the $[Fe^{II}(CN)_5(INH)]^{3-}$ against the malarial enzyme. This work investigates the efficacy of the $[Fe^{II}(CN)_5(INH)]^{3-}$ compound against PfENR. In addition, we propose an enzyme mechanism for PfENR based on steady-state kinetics, pre-steady-state kinetics, and fluorescence spectroscopy data.

2. Materials and Methods

2.1. Materials. All chemicals used were of analytical or reagent grade and required no further purification. Crotonoyl-CoA, NADH, and butyryl-CoA were from Sigma (Steinheim, Germany). PfENR (EC 1.3.1.9) was expressed and purified by Genscript Corp., New Jersey, USA. The $[Fe^{II}(CN)_5(INH)]^{3-}$ compound was a kind gift of Dr. Luiz G.F Lopes and Dr. Eduardo H.S. Sousa from Universidade Federal do Ceará, Departamento de Química Orgânica e Inorgânica, Fortaleza, CE, Brazil. The steady-state activity assays were carried out in a UV-2550 UV-Visible Spectrophotometer, and fluorescence binding experiments were carried out in an RF-5301PC Spectrophotometer, both from Shimadzu (Kyoto, Japan).

All enzyme activity assays were performed under initial rate conditions at 25°C in 100 mM sodium phosphate buffer pH 7.5 in $500\,\mu L$ total reaction volumes, and each individual initial rate datum was the average of duplicate or triplicate measurements. Crotonoyl-CoA, NADH, butyryl-CoA, $[Fe^{II}(CN)_5(INH)]^{3-}$, and the enzyme were dissolved in 100 mM sodium phosphate buffer pH 7.5. The reactions were monitored by the decrease in absorbance at 340 nm due to the conversion of NADH ($\varepsilon_{340} = 6220\,M^{-1}\,cm^{-1}$) to NAD^+.

2.2. Initial Velocity. In order to determine the true steady-state kinetic parameters and initial velocity patterns, PfENR activity was measured in the presence of varying concentrations of crotonoyl-CoA (10–240 μM) and several fixed-varied NADH concentrations (20–200 μM), and reactions were initiated by the addition of 0.12 μM of PfENR into the reaction mixture.

2.3. Fluorescence Spectroscopy. Fluorescence titration was performed to assess the dissociation constant at equilibrium for binary complexes formed between PfENR and either substrate(s) or product(s) at 25°C. Crotonoyl-CoA, NADH, butyryl-CoA, and PfENR were dissolved in 100 mM sodium phosphate buffer pH 7.5. Fluorescence titration with crotonoyl-CoA was carried out by making microliter additions of 0.5 mM and 5 mM crotonoyl-CoA stock solutions (0.50–425.97 μM crotonoyl-CoA final concentrations) to 1 mL of 3 μM PfENR, keeping the dilution to a maximum of 10.1%. Measurements of changes in intrinsic protein fluorescence of PfENR upon crotonoyl-CoA binding employed excitation wavelength at 305 nm, and the emission wavelengths ranged from 325 to 370 nm (maximum PfENR λ_{EM} = 348 nm); the slits for excitation and emission wavelengths were, respectively, 15 and 5 nm. Fluorescence titration with NADH was carried out by making microliter additions of 0.5 mM, 1 mM, and 5 mM NADH stock solutions (0.50–119.21 μM NADH final concentrations) to 1 mL of 3 μM PfENR, keeping the dilution to a maximum of 4.1%. Measurements of changes in NADH fluorescence upon binding to PfENR employed excitation wavelength at 360 nm, and the emission wavelengths ranged from 360 to 560 nm (maximum λ_{EM} = 460 nm); the slits for excitation and emission wavelengths were, respectively, 1.5 and 5 nm. Fluorescence titration with butyryl-CoA was carried out by making microliter additions of 0.5 mM, 2.5 mM, 5 mM, and 10 mM butyryl-CoA stock solutions (0.50–550.85 μM butyryl-CoA final concentrations) to 1 mL of 3 μM PfENR, keeping the dilution to a maximum of 8.4%. Measurements of changes in intrinsic protein fluorescence upon butyryl-CoA binding to PfENR employed excitation wavelength at 300 nm, and the emission wavelengths ranged from 320 to 400 nm (maximum PfENR λ_{EM} = 337 nm); the slits for excitation and emission wavelengths were, respectively, 5 and 10 nm. Control experiments were employed to both determine the maximum ligand concentrations to be used with no inner filter effect and determine dilution effects on protein fluorescence. No fluorescence titration with NAD^+ could be performed due to a large inner filter on protein fluorescence.

2.4. Pre-Steady-State Kinetics. Pre-steady-state kinetic measurements of NADH → NAD^+ conversion by PfENR were carried out to confirm the proposed kinetic mechanism and assess whether the apparent rate constant for this conversion contributes to the rate-limiting step. The decrease in absorbance upon NADH conversion to NAD^+ was monitored at 340 nm (1 mm slit width = 4.65 nm spectral band), at 25°C, using a split time base (0.2–2 s; 200 data points for each time base). The experimental conditions were 3.14 μM PfENR and 200 μM NADH in 100 mM sodium phosphate buffer pH 7.5 (mixing chamber concentrations). The dead time of the stopped-flow equipment is 1.37 ms.

2.5. $[Fe^{II}(CN)_5(INH)]^{3-}$ In Vitro Activity against PfENR. $[Fe^{II}(CN)_5(INH)]^{3-}$ time-dependent inhibition of PfENR was performed since it had been observed in MtInhA [31]. The enzyme was preincubated with the inhibitor for 15 min (2.77 : 2455 μM enzyme : inhibitor solution), and the activity was monitored by adding 0.12 : 54 μM enzyme : inhibitor mixture aliquots, with different times of exposure, to the reaction mixtures which contained crotonoyl-CoA and NADH concentrations close to their K_M values. The reaction was monitored by following enzyme activity during the time course.

2.6. Slow-Binding Inhibition Kinetics of PfENR by $[Fe^{II}(CN)_5 \cdot (INH)]^{3-}$. Typical slow-binding experiments were carried out in the presence of various $[Fe^{II}(CN)_5(INH)]^{3-}$ concentrations as an attempt to elucidate the kinetic mechanism of the time-dependent inhibition observed for PfENR. In the case of slow-binding inhibitors, the binding, which is comprised by the establishment of the equilibrium between enzyme, inhibitor, and enzyme-inhibitor complexes, occurs slowly in a time scale of seconds to minutes [32]. These experiments were conducted under conditions in which $[Fe^{II}(CN)_5(INH)]^{3-}$ concentrations were significantly larger than enzyme concentration, and measurements were made within a time range over which there was no significant substrate depletion. The assay mixtures contained 80 μM crotonoyl-CoA, 120 μM NADH, 2% (vol/vol) glycerol, 49.7 μg mL^{-1} BSA, and 0–35 μM $[Fe^{II}(CN)_5(INH)]^{3-}$. The reactions were initiated by adding enzyme (0.69 nM) to the assay mixture and were monitored by following the decrease in NADH absorbance at 340 nm for 21600 s (6 hours). Enzyme activity was stabilized by the addition of glycerol and BSA to the reaction mixture as described for MtInhA [25, 31].

2.7. Two-Step Mechanism of PfENR Inhibition by $[Fe^{II}(CN)_5 \cdot (INH)]^{3-}$. The two-step mechanism observed for MtInhA inhibition by $[Fe^{II}(CN)_5(INH)]^{3-}$ [31] was investigated for PfENR. The latter was preincubated in the presence of various concentrations of $[Fe^{II}(CN)_5(INH)]^{3-}$, and the decrease of PfENR activity was assessed by withdrawing aliquots from the preincubation mixtures at appropriate intervals, followed by rapid measurement of initial velocity. Reactions of time-dependent inactivation of PfENR were carried out in mixtures containing 12 μM PfENR and various concentrations of inhibitor. Control experiments were performed with no inhibitor. At various times, the residual enzyme activity was determined by diluting an aliquot (100-fold) of the reaction mixture into the assay solution, which contained 40 μM crotonoyl-CoA and 50 μM NADH.

2.8. Data Analysis. The kinetic parameter values and their respective standard errors were obtained by fitting the data to the appropriate equations by using the nonlinear regression function of SigmaPlot 2004 (SPSS, Inc.).

Apparently parallel family of lines of initial velocity data were tentatively fitted to (1), which describes a double displacement mechanism [33]. For (1), v is the measured reaction velocity, V is the maximal velocity, A and B are

the concentrations of the substrates (NADH and crotonoyl-CoA), and K_a and K_b are their respective Michaelis constants:

$$v = \frac{VAB}{K_aB + K_bA + AB}. \quad (1)$$

Data from equilibrium fluorescence spectroscopy were fitted either to a hyperbolic function ((2); [34]) or to the Hill equation ((3); [35]). For (2) and (3), F is the observed fluorescence signal, $F_{\max}$ is the maximal fluorescence, $F/F_{\max}$ ratio represents the degree of saturation, A is the concentration of the ligand (either NADH or butyryl-CoA), n represents the total number of binding sites, K_d is the overall dissociation constant, and K' represents a mean dissociation constant for enzyme: ligand binary complex formation, which is comprised of interaction factors and the intrinsic dissociation constant [36, 37]:

$$\frac{F}{F_{\max}} = \frac{A}{K_d + A}, \quad (2)$$

$$\frac{F}{F_{\max}} = \frac{A^n}{K' + A^n}. \quad (3)$$

The equilibrium fluorescence data representing the fractional saturation (0.10–0.90) for the homotetrameric form [38] of PfENR were fitted to (4) (the Hill plot), in which Y is the fraction of substrate binding sites occupied by the substrate and h is the Hill coefficient:

$$\log\left(\frac{Y}{1-Y}\right) = h\log A - \log K'. \quad (4)$$

The pre-steady-state time course of NADH $\rightarrow$ NAD^+ conversion was fitted to (5) for a single exponential decay, in which A is the absorbance at time t, A_0 is the absorbance at time zero, and k is the apparent first-order rate constant for product formation:

$$A = A_0 e^{-kt}. \quad (5)$$

Apparent pseudofirst-order rate constants were calculated by fitting the progress curves for time-dependent inactivation of PfENR to integrated equation (5) for slow-binding inhibition [25, 32, 39]. For (6), A_t and A_0 are the 340-nm absorbances at time t and time 0, v_0, v_s, and k_{obs} represent, respectively, the initial velocity, the final steady-state velocity, and the apparent first-order rate constant for the establishment of the equilibrium between EI and EI* complexes (the observed rate constant for formation of EI* or the apparent isomerization rate constant):

$$A_t = v_s t + \frac{(v_0 - v_s)\left(1 - e^{-k_{\text{obs}}t}\right)}{k_{\text{obs}}}. \quad (6)$$

An estimate of the apparent dissociation constant (K_i^{app}) was obtained by fitting the variation of initial rate (v_0) with inhibitor concentration (I) to (7) for competitive inhibition, in which $v_{0\max}$ is the initial velocity in the absence of inhibitor [31]:

$$v_0 = \frac{v_{0\max}}{1 + [I]/K_i^{\text{app}}}. \quad (7)$$

A "true" value for the apparent dissociation constant K_i for the initial enzyme-inhibitor binary complex (EI) can be calculated by (8), in which K_{NADH} and $K_{\text{Crotonoyl-CoA}}$ are the values for the Michaelis-Menten constants and [NADH] and [Crotonoyl-CoA] are the concentration values used in the slow-onset inhibition assays:

$$K_i = \frac{K_i^{\text{app}}}{1 + [\text{NADH}]/K_{\text{NADH}} + [\text{Crotonoyl-CoA}]/K_{\text{Crotonoyl-CoA}}}. \quad (8)$$

The data from two-step mechanism studies of PfENR inhibition by $[Fe^{II}(CN)_5(INH)]^{3-}$ were fitted to (9), in which K_i is the dissociation constant for the initial enzyme-inhibitor binary complex (EI), k_5 is the forward isomerization rate constant for conversion of EI to EI*, k_6 is the reverse isomerization rate constant (conversion of EI* to EI), I is the concentration of inhibitor ($[Fe^{II}(CN)_5(INH)]^{3-}$), and k_{inact} is the apparent first-order constant for enzyme inhibition:

$$k_{\text{inact}} = k_6 + \frac{k_5 I}{K_i + I}. \quad (9)$$

3. Results and Discussion

3.1. Initial Velocity Patterns and Kinetic Constants. Initial velocity patterns were determined using either crotonoyl-CoA or NADH as the variable substrate to distinguish between a sequential and a double displacement ("ping-pong") mechanism, providing information regarding the order of substrate binding. Double-reciprocal plot [40] analysis revealed a parallel line pattern for both substrates (Figure 3), which is consistent with a double displacement mechanism. In this mechanism, a catalytic event can occur when only one of the two substrates is bound to the enzyme. A catalytic event occurs after the binding of substrate A to the enzyme (E), but prior to the binding of substrate B. After the first catalytic event, a portion of substrate A remains in the active site of the enzyme, whereas the other portion denoted as product P dissociates. The first catalytic event produces a different stable enzyme form (F) to which substrate B can bind and proceed with catalysis to generate product Q and regenerate free enzyme (E). The data were tentatively fitted to (1), yielding the following values for the true steady-state kinetic constants: $V_{\max} = 5.8\ (\pm 0.3)\ \text{U mg}^{-1}$, $k_{\text{cat}} = 6.2\ (\pm 0.4)\ \text{s}^{-1}$, $K_{\text{NADH}} = 85\ (\pm 9)\ \mu\text{M}$, $K_{\text{Crotonoyl-CoA}} = 63\ (\pm 6)\ \mu\text{M}$, $k_{\text{cat}}/K_{\text{NADH}} = 7.3\ (\pm 0.9) \times 10^4\ \text{M}^{-1}\ \text{s}^{-1}$, and $k_{\text{cat}}/K_{\text{Crotonoyl-CoA}} = 9.8\ (\pm 1.1) \times 10^4\ \text{M}^{-1}\ \text{s}^{-1}$.

There are, however, some conditions where lines that seem parallel really are not. For an Ordered Bi Bi system in which the dissociation constant for substrate A (K_{ia}) is very much smaller than the Michaelis-Menten constant for A (K_a or K_{MA}), the family of reciprocal plots intersect far to the left of the $1/v$ axis and far below the 1/[A] axis [36]. In addition, seemingly parallel initial velocity patterns can also occur in rapid equilibrium random systems where the binding of one substrate strongly inhibits the binding of the other.

3.2. Equilibrium Binding of Ligands to PfENR. Equilibrium binary complex formation experiments were employed to

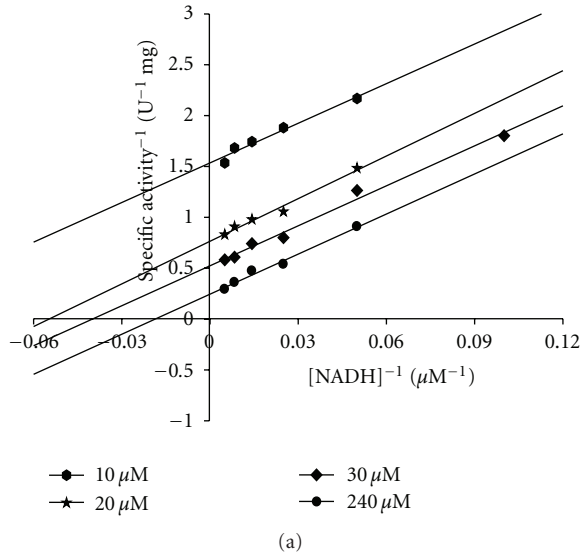

(a)

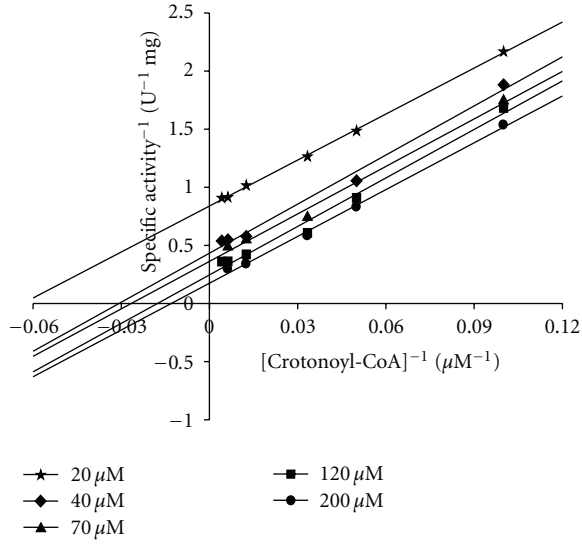

(b)

Figure 3: Intersecting initial velocity patterns for PfENR with either NADH (a) or crotonoyl-CoA (b) as the variable substrate. Each curve represents varied-fixed levels of the cosubstrate: one unit of enzyme activity (U) is defined as the amount of enzyme that catalyses the phosphorolysis of 1 μmol of crotonoyl-CoA per minute in a 1 cm optical path.

confirm, or refute, the proposed enzyme mechanism. There was an enhancement in nucleotide fluorescence upon NADH binding to PfENR, whereas butyryl-CoA binding to PfENR resulted in intrinsic protein fluorescence quench. Titration of PfENR with NADH was hyperbolic (Figure 4(a)), and the data were fitted to (3) yielding a value of 398 ($\pm$53) μM for the overall dissociation constant (K_d) of NADH. Enzyme titration with butyryl-CoA was sigmoidal (Figure 4(b)), and the data were best fitted to (4) yielding a value for K' for butyryl-CoA of 1151 ($\pm$638) μM. The value for K' represents a mean dissociation constant for PfENR : butyryl-CoA binary complex formation, which is comprised of interaction

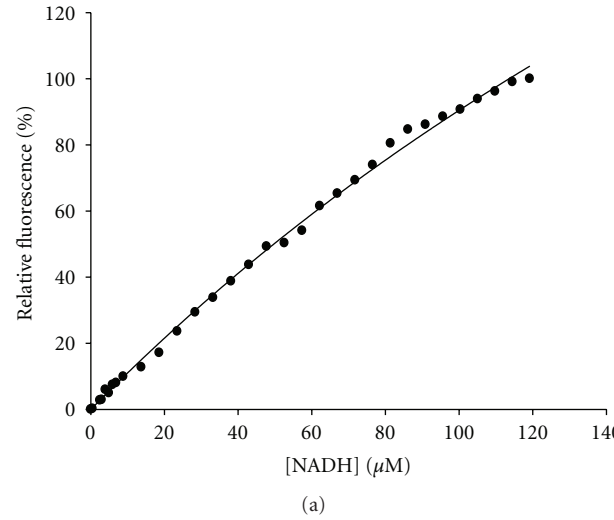

(a)

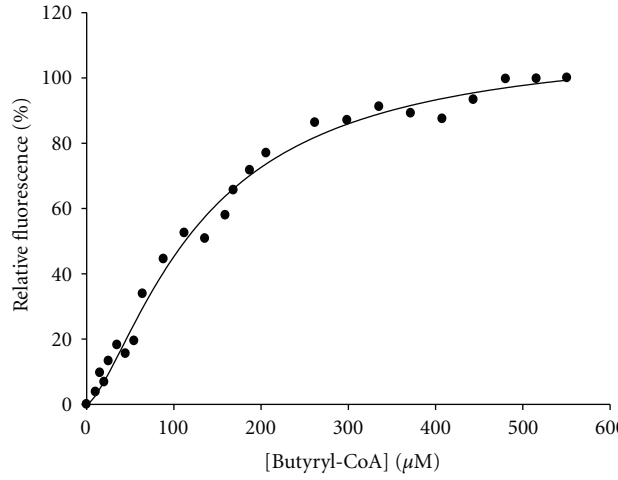

(b)

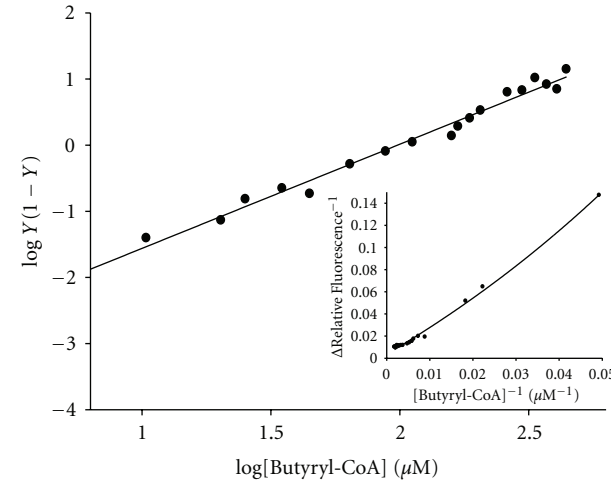

(c)

Figure 4: Overall dissociation constant for PfENR: NADH (a) and PfENR : butyryl-CoA (b) binary complex formation monitoring changes in, respectively, nucleotide and intrinsic protein fluorescence. (c) Hill logarithmic plot of the data between 10% and 90% active site saturation with butyryl-CoA. Inset represents the fit of double-reciprocal plot of the fluorescence data to an exponential growth equation.

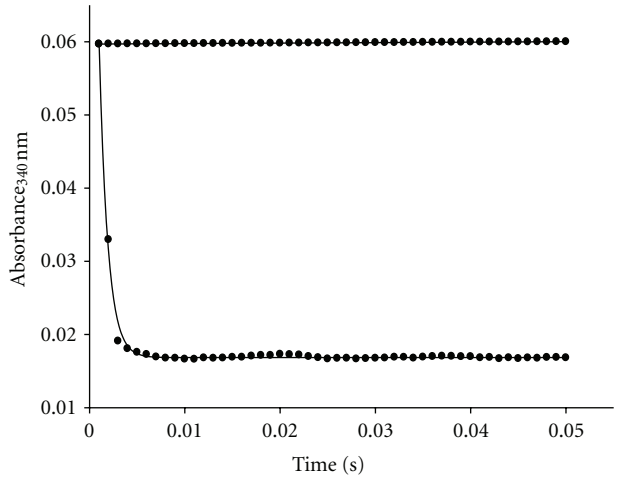

FIGURE 5: Representative stopped-flow trace for NADH → NAD^+ conversion. Fitting the exponential decay data to (5) yielded a value of 1100 (±29) s^{-1} for the apparent first-order rate constant of product formation. The top trace represents the chemical control (200 μM NADH), and the single exponential decay represents the reaction upon mixing 3.14 μM PfENR and 200 μM NADH (mixing chamber concentrations).

factors and the intrinsic dissociation constant [36, 37]. A Hill plot of the data (Figure 4(c)) fitted to (4) yielded a value larger than one for h (1.6 ± 0.1). The latter indicates moderate positive homotropic cooperativity on butyryl-CoA binding to tetrameric PfENR, which is further supported by the upward-curved double-reciprocal plot (Figure 4(c)—inset). No intrinsic protein fluorescence change upon addition of crotonoyl-CoA to PfENR could be observed, suggesting that this compound cannot bind to free PfENR enzyme. Protein fluorescence titration with NAD^+ could not be performed due to large inner filter effect.

3.3. Pre-Steady-State Kinetics. Steady-state kinetics data suggested that PfENR follows a double displacement ("ping-pong") mechanism. Fluorescence spectroscopy data showed that NADH binds to free enzyme whereas it appears that crotonoyl-CoA cannot. Although butyryl-CoA binding to free enzyme resulted in protein fluorescence quench, it is not certain whether crotonoyl-CoA cannot bind to free enzyme or its binding results in no change in protein fluorescence. Hence, the Ordered Bi Bi and rapid equilibrium random mechanisms could not be ruled out. To try to address this uncertainty, pre-steady-state kinetics measurements were carried out to show whether or not there is hydride transfer in the absence of crotonoyl-CoA as expected for the double displacement mechanism with NADH binding first. Moreover, determination of a value for the apparent first-order rate constant for the course of NADH → NAD^+ conversion could also indicate whether or not this step is rate limiting. It should be pointed out that NADH concentration was in excess as compared to PfENR concentration, so that any burst in product formation could be reliably assessed [41, 42]. Fitting the pre-steady-state trace showing a single exponential decay upon NADH → NAD^+ conversion (Figure 5) to (5) yielded a value of 1100 (±29) s^{-1} for the apparent first-order rate constant for product formation (1 cm pathlength). The NADH → NAD^+ conversion step has thus no contribution to rate-limiting step(s) as its value is much larger than the catalytic rate constant value. There was an apparent accumulation of observable product (NAD^+) on the enzyme active sites when high concentration of PfENR (3.14 μM) was mixed with NADH (200 μM). Taken together, steady-state kinetics, pre-steady-state kinetics, and equilibrium binding data are consistent with a double displacement mechanism for PfENR (Figure 6). In this mechanism, a catalytic event occurs after the binding of NADH to free enzyme (E), generating and releasing NAD^+ into solution prior to the binding of crotonoyl-CoA to a modified form of the enzyme (F), followed by formation of butyryl-CoA and regeneration of free enzyme (E) (Figure 6). The enzyme mechanism has been shown to be ordered sequential with enoyl-ACP substrate binding first for *Staphylococcus aureus* enoyl reductase [43] and ordered sequential with NADH binding first for *fabV*-encoded enoyl reductase from *Burkholderia mallei* [44]. Although uncommon for reductases/dehydrogenases, double displacement mechanisms have been described for *Enterobacter cloacae* nitroreductase [45], *Salmonella typhimurium* histidinol dehydrogenase [46], bovine liver mitochondrial dihydroorotate dehydrogenase [47], and mammalian pyruvate dehydrogenase complex [48]. Of course, no mechanism is ever proved; at best one can say that given the current data the likely mechanism for PfENR is double displacement. Further efforts are needed to provide support for either the double displacement mechanism or any other that may give a better description of the experimental results.

Based on substrate binding to immobilized PfENR by Surface Plasmon Resonance (SPR) results, it has been proposed that PfENR enzyme mechanism is random order of substrate addition [49]. Although there have been reports on determination of apparent steady-state kinetics parameters for PfENR [38, 50, 51], to the best of our knowledge, no data have been presented for determination of true steady-state kinetic parameters on which to base a proposal for PfENR enzyme mechanism in solution. To determine the true steady-state kinetic parameters and initial velocity patterns for distinguishing mechanisms, enzyme activity measurements have to be carried out in the presence of varying concentrations of one substrate and several fixed-varied concentrations of the other substrate. Interestingly, the K_d value of 398 μM for NADH is approximately 8-fold larger than a previously reported value (51.6 μM) by SPR [49]. These results are somewhat puzzling as equilibrium constants determined by SPR usually match well the values obtained by solution techniques (fluorescence spectroscopy, isothermal titration calorimetry). In addition, a K_d value of 62.5 μM for crotonoyl-CoA has been determined by SPR measurements [49], whereas no change in intrinsic PfENR protein fluorescence could be detected upon addition of crotonoyl-CoA to free enzyme. Incidentally, the true steady-state value for k_{cat} (6.2 s^{-1}) reported here is approximately

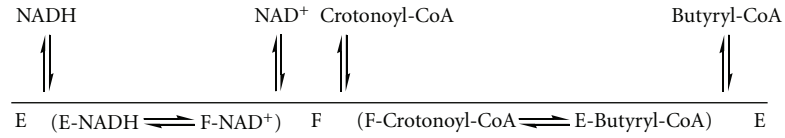

Figure 6: Proposed mechanism for the PfENR-catalysed chemical reaction.

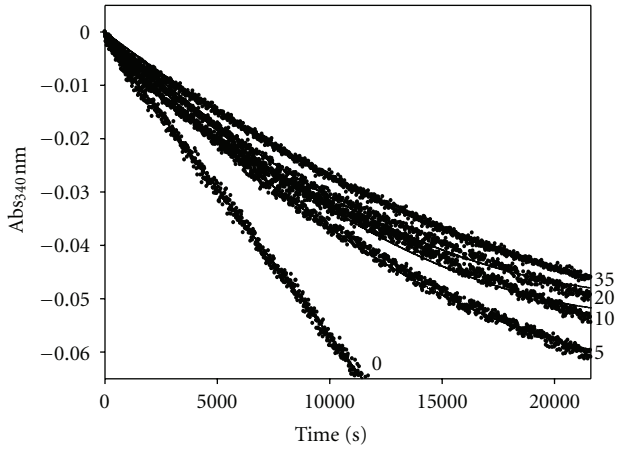

Figure 7: Time-dependent inactivation of PfENR by 0–35 μM $[Fe^{II}(CN)_5(INH)]^{3-}$. The solid curves represent the best fit of the data to (5) for slow-binding inhibition. The assay mixtures were kept at 25°C and contained 100 mM sodium phosphate buffer pH 7.5, 80 μM crotonoyl-CoA, 120 μM NADH, 2% (vol/vol) glycerol, 49.7 μg mL^{-1} BSA, and 0–35 μM $[Fe^{II}(CN)_5(INH)]^{3-}$. The reactions were initiated by the addition of enzyme (0.69 nM) to the assay mixture and were monitored by following the decrease in NADH absorbance at 340 nm for 21600 s (6 hours).

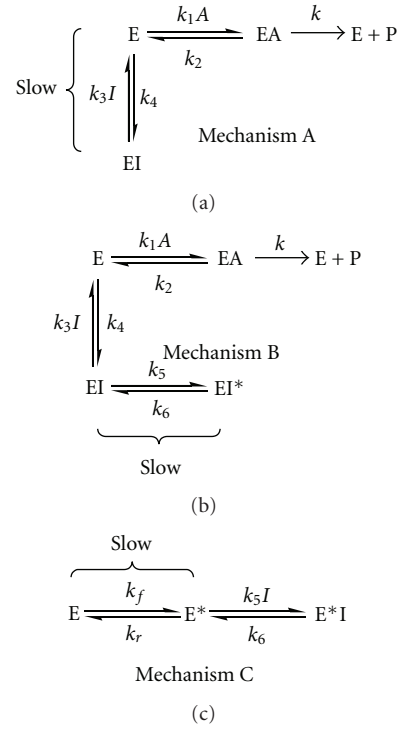

Figure 8: Mechanisms that describe reversible slow-binding inhibition of enzyme-catalysed reactions.

4-fold larger as compared to an apparent value (1.62 s^{-1}) described elsewhere [51].

3.4. Slow-Onset Inhibition Kinetics of PfENR by $[Fe^{II}(CN)_5 \cdot (INH)]^{3-}$. We have previously shown that $[Fe^{II}(CN)_5 \cdot (INH)]^{3-}$ compound (Figure 2(b)) is a slow-onset inhibitor of wild-type and drug-resistant MtInhAs [30, 31, 52]. We then anticipated that $[Fe^{II}(CN)_5(INH)]^{3-}$ may also be an effective inhibitor of PfENR enzyme activity. Prior to embarking on a full analysis of the mode of inhibition of PfENR activity by $[Fe^{II}(CN)_5(INH)]^{3-}$ compound, the enzyme was preincubated with inhibitor, and aliquots were withdrawn at different times to measure the remaining residual activity. PfENR inhibition by $[Fe^{II}(CN)_5(INH)]^{3-}$ was time dependent (data not shown). Thereby, PfENR slow-binding experiments were carried out in the presence of various concentrations of $[Fe^{II}(CN)_5(INH)]^{3-}$ to try to elucidate the mechanism of the observed time-dependent enzyme inhibition. The progress curves for enzyme activity indicate that $[Fe^{II}(CN)_5(INH)]^{3-}$ is a slow-onset inhibitor of PfENR (Figure 7).

Three basic slow-onset inhibition mechanisms have been described by Morrison and Walsh (Figure 8; [32]).

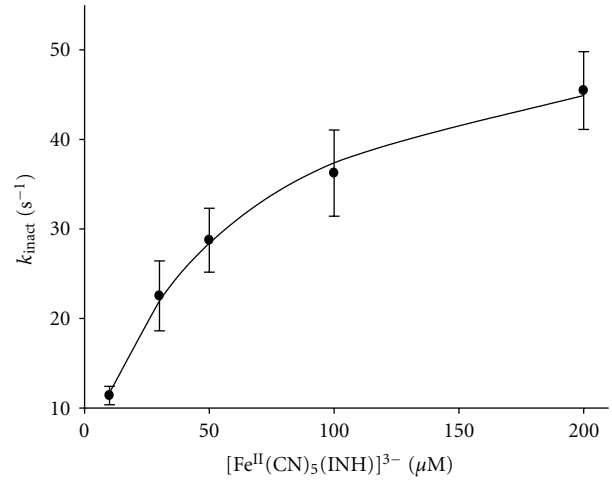

Figure 9: Two-step inactivation of PfENR by $[Fe^{II}(CN)_5(INH)]^{3-}$. The values for the apparent first-order rate constant of inactivation (k_{inact}) were obtained from a plot of residual enzyme activity versus time (not shown). The k_{inact} values were plotted against $[Fe^{II}(CN)_5(INH)]^{3-}$ concentration in the preincubation mixture. The data were fitted to (6).

In mechanism A (Figure 8), it is assumed that the time-dependent enzyme inactivation observed is resultant of a slow bimolecular enzyme-inhibitor interaction, because the inhibitor concentration is low and/or due to barriers that the inhibitor encounters in its binding at the enzyme's active site. In mechanism B (Figure 8), it is assumed that there is an initial rapid enzyme-inhibitor interaction to form EI, which then undergoes a slow isomerization (conformational change) to EI* [53]. For inhibitors that conform to this mechanism, the overall dissociation constant (K_i^*) must be lower than the dissociation constant for initially formed complex EI (K_i), a condition that can be satisfied only when $k_6 < k_5$ ($K_i^* = K_i k_6/(k_5 + k_6)$) and when k_5 and k_6 are slower than all other steps [32]. According to mechanism B, in the presence of a fixed concentration of substrate (A), the value of k_{obs} increases hyperbolically as a function of inhibitor concentration with limiting values of k_6 and $k_5 + k_6$ at, respectively, zero and infinite concentrations of inhibitor. As described in Section 2, k_{obs} in (6) represents the apparent first-order rate constant for the establishment of the equilibrium between EI and EI* complexes (the observed rate constant for formation of EI* or the apparent isomerization rate constant). A third mechanism (mechanism C) has also been described to account for slow-binding inhibition of enzyme-catalysed reactions (Figure 8). This mechanism involves a slow initial isomerization of two forms of free enzyme in solution (E and E*), followed by a rapid binding of inhibitor to form E*I complex. The k_f and k_r stand, respectively, for the forward and reverse rate constants for the conversion of free enzyme (E) to a form of free enzyme (E*) to which the inhibitor binds. However, fitting the k_{obs} values as a function of $[Fe^{II}(CN)_5(INH)]^{3-}$ inhibitor concentration yielded a plot that did not allow to draw solid conclusions on the mechanism. On the other hand, fitting the initial rate values (v_0) as a function of $[Fe^{II}(CN)_5(INH)]^{3-}$ inhibitor concentration to (7) yielded a value of 40 (± 11) μM for K_i^{app}. A "true" value of 11 (± 3) μM for the apparent dissociation constant K_i for the initial enzyme-inhibitor binary complex (EI) could thus be calculated by employing (8).

3.5. Two-Step Mechanism of PfENR Inhibition by $[Fe^{II}(CN)_5 \cdot (INH)]^{3-}$. The two-step mechanism of PfENR inhibition by $[Fe^{II}(CN)_5(INH)]^{3-}$ was assessed by an experiment in which the enzyme was preincubated in the presence of various concentrations of inhibitor and the decrease of PfENR activity was assessed by withdrawing aliquots of enzyme from preincubation mixtures at appropriate intervals, followed by rapid measurement of initial velocity. These results were analyzed in terms of a two-step inhibition mechanism in which the initial rapid binding of the inhibitor to enzyme is followed by a second slow step that results in the final enzyme-inhibitor complex. Since the value of K_i is much larger than K_i^*, the inhibitor concentration in the assay solution is lower than the K_i value ($[I] < K_i$), and there is a large excess of the competitive substrates NADH and crotonoyl-CoA over $[Fe^{II}(CN)_5(INH)]^{3-}$, the steady-state concentration of EI in the assay solution is kinetically insignificant [31]. The apparent first-order rate constants for PfENR inactivation (k_{inact}) could be calculated from a plot of residual enzyme activity against time for each inhibitor concentration. A plot of k_{inact} values versus inhibitor concentration shows that the k_{inact} values increase hyperbolically as a function of inhibitor concentration (Figure 9), which is consistent with mechanism B (Figure 8). These data were thus fitted to (9), which describes the slow-binding inhibition for mechanism B, yielding values of 58 (± 12) μM for K_i, 53 (± 2) s^{-1} for k_5, and 4 (± 2) s^{-1} for k_6. A value of 4 μM can thus be calculated for the overall inhibition constant ($K_i^* = K_i k_6/(k_5 + k_6)$). It should be pointed out that an independent estimate for the K_i^* value could be obtained by plotting the final steady-state velocity (v_s) as a function of $[Fe^{II}(CN)_5(INH)]^{3-}$ inhibitor concentration and fitting the data to (7) for competitive inhibition. However, the data were not consistent as the experimental data appear to depart somewhat from the values predicted by fitting the data to (6).

The two-step mechanism followed by $[Fe^{II}(CN)_5 \cdot (INH)]^{3-}$ inactivation of PfENR involves an enzyme-inhibitor isomerization step. The enzyme isomerization could involve, for instance, a protein conformational change or alteration of water structure at the active site. For the inhibitor, the change could be hydration/dehydration of a carbonyl, change in ionization state, or a conformational change. These alterations could take place in the enzyme-inhibitor complex or in solution [54].

4. Concluding Remarks

The weakness in the use of classical enzyme inhibitors as drugs for clinical conditions is that inhibition results in the upstream accumulation of the substrate for the enzyme, which may overcome the inhibition. By contrast, the build-up of substrate cannot have any effect on the isomerization of enzyme-inhibitor complex typical of the slow-onset mechanism and hence reversal of the inhibition [32]. Moreover, the low half-time value for the limiting step for inhibitor dissociation from the binary complex is a desirable feature since it may be expected to enhance inhibitor's effectiveness [54]. It has recently been proposed by scientists at GlaxoSmithKline (USA) that measurement of the dissociative half-life is a crucial metric of compound optimization and could be a key indicator of *in vivo* duration of efficacy and target selectivity [55]. It has recently been shown that $[Fe^{II}(CN)_5(INH)]^{3-}$ compound has a promising profile in toxicological assays and that it is amenable to large-scale production [56]. These features indicate that $[Fe^{II}(CN)_5(INH)]^{3-}$ compound is a viable candidate for further studies (including *in vivo* efficacy) and that it may represent a prototype for the development of chemotherapeutic agents to treat malaria.

Acknowledgments

This work was supported by Millennium Initiative Program (CNPq), Brazil, to L. H. P. Silva The authors also

acknowledge support by National Institute of Science and Technology on Tuberculosis (Decit/SCTIE/MS-MCT-CNPq-FNDCT-CAPES). P. S. M. Medeiros and R. G. Ducati thank fellowships awarded by CNPq.

References

[1] WHO, World Health Organization, "10 Facts on malaria," WHO, Geneva, Switzerland, 2009, http://www.who.int/features/factfiles/malaria/en/index.html.

[2] S. I. Hay, C. A. Guerra, A. J. Tatem, P. M. Atkinson, and R. W. Snow, "Urbanization, malaria transmission and disease burden in Africa," *Nature Reviews Microbiology*, vol. 3, no. 1, pp. 81–90, 2005.

[3] D. C. Warhurst, "Antimalarial drugs. An update," *Drugs*, vol. 33, no. 1, pp. 50–65, 1987.

[4] H. C. Spencer, W. W. Watkins, D. G. Sixsmith, and D. K. Koech, "Response of *Plasmodium falciparum* to dihydrofolate reductase inhibitors in Malindi, Kenya," *Transactions of the Royal Society of Tropical Medicine and Hygiene*, vol. 80, no. 2, pp. 201–203, 1986.

[5] J. H. McKie, K. T. Douglas, C. Chan et al., "Rational drug design approach for overcoming drug resistance: application to pyrimethamine resistance in malaria," *Journal of Medicinal Chemistry*, vol. 41, no. 9, pp. 1367–1370, 1998.

[6] N. M. Carballeira, "New advances in fatty acids as antimalarial, antimycobacterial and antifungal agents," *Progress in Lipid Research*, vol. 47, no. 1, pp. 50–61, 2008.

[7] C. Wongsrichanalai, A. L. Pickard, W. H. Wernsdorfer, and S. R. Meshnick, "Epidemiology of drug-resistant malaria," *Lancet Infectious Diseases*, vol. 2, no. 4, pp. 209–218, 2002.

[8] P. Piola, C. Fogg, F. Bajunirwe et al., "Supervised versus unsupervised intake of six-dose artemether-lumefantrine for treatment of acute, uncomplicated *Plasmodium falciparum* malaria in Mbarara, Uganda: a randomised trial," *The Lancet*, vol. 365, no. 9469, pp. 1467–1473, 2005.

[9] G. I. McFadden and D. S. Roos, "Apicomplexan plastids as drug targets," *Trends in Microbiology*, vol. 7, no. 8, pp. 328–333, 1999.

[10] R. F. Waller, P. J. Keeling, R. G. K. Donald et al., "Nuclear-encoded proteins target to the plastid in *Toxoplasma gondii* and *Plasmodium falciparum*," *Proceedings of the National Academy of Sciences of the United States of America*, vol. 95, no. 21, pp. 12352–12357, 1998.

[11] S. A. Ralph, G. G. van Dooren, R. F. Waller et al., "Metabolic maps and functions of the *Plasmodium falciparum* apicoplast," *Nature Reviews Microbiology*, vol. 2, no. 3, pp. 203–216, 2004.

[12] D. Tasdemir, "Type II fatty acid biosynthesis, a new approach in antimalarial natural product discovery," *Phytochemistry Reviews*, vol. 5, no. 1, pp. 99–108, 2006.

[13] H. J. Vial, P. Eldin, A. G. M. Tielens, and J. J. van Hellemond, "Phospholipids in parasitic protozoa," *Molecular and Biochemical Parasitology*, vol. 126, no. 2, pp. 143–154, 2003.

[14] P. Sinnis and B. K. L. Sim, "Cell invasion by the vertebrate stages of *Plasmodium*," *Trends in Microbiology*, vol. 5, no. 2, pp. 52–58, 1997.

[15] C. O. Rock and J. E. Cronan, "*Escherichia coli* as a model for the regulation of dissociable (type II) fatty acid biosynthesis," *Biochimica et Biophysica Acta*, vol. 1302, no. 1, pp. 1–16, 1996.

[16] N. Surolia and A. Surolia, "Triclosan offers protection against blood stages of malaria by inhibiting enoyl-ACP reductase of *Plasmodium falciparum*," *Nature Medicine*, vol. 7, no. 2, pp. 167–173, 2001.

[17] G. Weeks and S. J. Wakil, "Studies on the mechanism of fatty acid synthesis. 18. Preparation and general properties of the enoyl acyl carrier protein reductases from *Escherichia coli*," *The Journal of Biological Chemistry*, vol. 243, no. 6, pp. 1180–1189, 1968.

[18] A. Banerjee, E. Dubnau, A. Quemard et al., "*inhA*, a gene encoding a target for isoniazid and ethionamide in *Mycobacterium tuberculosis*," *Science*, vol. 263, no. 5144, pp. 227–230, 1994.

[19] K. Johnson, D. S. King, and P. G. Schultz, "Studies on the mechanisms of action of isoniazid and ethionamide in the chemotherapy of tuberculosis," *Journal of the American Chemical Society*, vol. 117, no. 17, pp. 5009–5010, 1995.

[20] K. Johnsson and P. G. Schultz, "Mechanistic studies of the oxidation of isoniazid by the catalase peroxidase from *Mycobacterium tuberculosis*," *Journal of the American Chemical Society*, vol. 116, no. 16, pp. 7425–7426, 1994.

[21] B. Heym, P. M. Alzari, N. Honoré, and S. T. Cole, "Missense mutations in the catalase-peroxidase gene, katG, are associated with isoniazid resistance in *Mycobacterium tuberculosis*," *Molecular Microbiology*, vol. 15, no. 2, pp. 235–245, 1995.

[22] S. V. Ramaswamy, R. Reich, S. J. Dou et al., "Single nucleotide polymorphisms in genes associated with isoniazid resistance in *Mycobacterium tuberculosis*," *Antimicrobial Agents and Chemotherapy*, vol. 47, no. 4, pp. 1241–1250, 2003.

[23] D. A. Rozwarski, G. A. Grant, D. H. R. Barton, W. R. Jacobs, and J. C. Sacchettini, "Modification of the NADH of the isoniazid target (InhA) from *Mycobacterium tuberculosis*," *Science*, vol. 279, no. 5347, pp. 98–102, 1998.

[24] B. Lei, C. J. Wei, and S. C. Tu, "Action mechanism of antitubercular isoniazid: activation by *Mycobacterium tuberculosis* KatG, isolation, and characterization of InhA inhibitor," *The Journal of Biological Chemistry*, vol. 275, no. 4, pp. 2520–2526, 2000.

[25] R. Rawat, A. Whitty, and P. J. Tonge, "The isoniazid-NAD adduct is a slow, tight-binding inhibitor of InhA, the *Mycobacterium tuberculosis* enoyl reductase: adduct affinity and drug resistance," *Proceedings of the National Academy of Sciences of the United States of America*, vol. 100, no. 2, pp. 13881–13886, 2003.

[26] R. S. Magliozzo and J. A. Marcinkeviciene, "The role of Mn(II)-peroxidase activity of mycobacterial catalase- peroxidase in activation of the antibiotic isoniazid," *The Journal of Biological Chemistry*, vol. 272, no. 14, pp. 8867–8870, 1997.

[27] S. Chouchane, S. Girotto, S. Yu, and R. S. Magliozzo, "Identification and characterization of tyrosyl radical formation in *Mycobacterium tuberculosis* catalase-peroxidase (KatG)," *The Journal of Biological Chemistry*, vol. 277, no. 45, pp. 42633–42638, 2002.

[28] M. Wilming and K. Johnsson, "Spontaneous formation of the bioactive form of the tuberculosis drug isoniazid," *Angewandte Chemie*, vol. 38, no. 17, pp. 2588–2590, 1999.

[29] M. Nguyen, A. Quemard, H. Marrakchi, J. Bernadou, and B. Meunier, "The nonenzymatic activation of isoniazid by Mn^{III}-pyrophosphate in the presence of NADH produces the inhibition of the enoyl-ACP reductase InhA from *Mycobacterium tuberculosis*," *Comptes Rendus de l'Academie des Sciences—Series IIc*, vol. 4, no. 1, pp. 35–40, 2001.

[30] J. S. Oliveira, E. H. S. Sousa, L. A. Basso et al., "An inorganic iron complex that inhibits wild-type and an isoniazid-resistant mutant 2-*trans*-enoyl-ACP (CoA) reductase from *Mycobacterium tuberculosis*," *Chemical Communications*, vol. 10, no. 3, pp. 312–313, 2004.

[31] J. S. Oliveira, E. H. S. de Sousa, O. N. de Souza, I. S. Moreira, D. S. Santos, and L. A. Basso, "Slow-onset inhibition of 2-trans-enoyl-ACP (CoA) reductase from *Mycobacterium tuberculosis* by an inorganic complex," *Current Pharmaceutical Design*, vol. 12, no. 19, pp. 2409–2424, 2006.

[32] J. F. Morrison and C. T. Walsh, "The behavior and significance of slow-binding enzyme inhibitors," *Advances in enzymology and related areas of molecular biology*, vol. 61, pp. 201–301, 1988.

[33] H. J. Smith and C. Simons, *Enzymes and Their Inhibition: Drug Development*, CRC Enzyme Inhibitors Series, CRC Press, Boca Raton, Fla, USA, 2005.

[34] L. Michaelis and M. L. Menten, "Die Kinetic der Invertinwirkung," *Biochemische Zeitschrift*, vol. 49, pp. 333–369, 1913.

[35] A.V. Hill, "The combinations of haemoglobin with oxygen and with carbon monoxide," *Biochemical Journal*, vol. 7, no. 5, pp. 471–480, 1913.

[36] I. H. Segel, *Enzyme Kinetics. Behavior and Analysis of Rapid Equilibrium and Steady-State Enzyme Systems*, John Wiley & Sons, New York, NY, USA, 1975.

[37] G. Weber, "Energetics of ligand binding to proteins," *Advances in Protein Chemistry*, vol. 29, pp. 1–83, 1975.

[38] M. Kapoor, J. Gopalakrishnapai, N. Surolia, and A. Surolia, "Mutational analysis of the triclosan-binding region of enoyl-ACP (acyl-carrier protein) reductase from *Plasmodium falciparum*," *Biochemical Journal*, vol. 381, no. 3, pp. 735–741, 2004.

[39] W. Liu, C. J. Rogers, A. J. Fisher, and M. D. Toney, "Aminophosphonate inhibitors of dialkylglycine decarboxylase: structural basis for slow binding inhibition," *Biochemistry*, vol. 41, no. 41, pp. 12320–12328, 2002.

[40] H. Lineweaver and D. Burk, "The determination of enzyme dissociation constants," *Journal of the American Chemical Society*, vol. 56, no. 3, pp. 658–666, 1934.

[41] K. Hiromi, *Kinetics of Fast Enzyme Reactions: Theory and Practice*, Kodansha, 1979.

[42] L. A. Basso, P. C. Engel, and A. R. Walmsley, "The mechanism of substrate and coenzyme binding to clostridial glutamate dehydrogenase during reductive amination," *European Journal of Biochemistry*, vol. 234, no. 2, pp. 603–615, 1995.

[43] H. Xu, T. J. Sullivan, J. I. Sekiguchi et al., "Mechanism and inhibition of saFabI, the enoyl reductase from *Staphylococcus aureus*," *Biochemistry*, vol. 47, no. 14, pp. 4228–4236, 2008.

[44] H. Lu and P. J. Tonge, "Mechanism and inhibition of the FabV Enoyl-ACP reductase from *Burkholderia mallei*," *Biochemistry*, vol. 49, no. 6, pp. 1281–1289, 2010.

[45] R. L. Koder and A. F. Miller, "Steady-state kinetic mechanism, stereospecificity, substrate and inhibitor specificity of *Enterobacter cloacae* nitroreductase," *Biochimica et Biophysica Acta*, vol. 1387, no. 1-2, pp. 395–405, 1998.

[46] H. Görisch, "Steady-state investigations of the mechanism of histidinol dehydrogenase," *Biochemical Journal*, vol. 181, no. 1, pp. 153–157, 1979.

[47] V. Hines and M. Johnston, "Analysis of the kinetic mechanism of the bovine liver mitochondrial dihydroorotate dehydrogenase," *Biochemistry*, vol. 28, no. 3, pp. 1222–1226, 1989.

[48] C. S. Tsai, M. W. Burgett, and L. J. Reed, "α Keto acid dehydrogenase complexes. XX. A kinetic study of the pyruvate dehydrogenase complex from bovine kidney," *The Journal of Biological Chemistry*, vol. 248, no. 24, pp. 8348–8352, 1973.

[49] M. Kapoor, P. L. S. Mukhi, N. Surolia, K. Suguna, and A. Surolia, "Kinetic and structural analysis of the increased affinity of enoyl-ACP (acyl-carrier protein) reductase for triclosan in the presence of NAD^+ ," *Biochemical Journal*, vol. 381, no. 3, pp. 725–733, 2004.

[50] R. Perozzo, M. Kuo, A. B. S. Sidhu et al., "Structural elucidation of the specificity of the antibacterial agent triclosan for malarial enoyl acyl carrier protein reductase," *The Journal of Biological Chemistry*, vol. 277, no. 15, pp. 13106–13114, 2002.

[51] M. Kapoor, M. J. Dar, A. Surolia, and N. Surolia, "Kinetic determinants of the interaction of enoyl-ACP reductase from *Plasmodium falciparum* with its substrates and inhibitors," *Biochemical and Biophysical Research Communications*, vol. 289, no. 4, pp. 832–837, 2001.

[52] I. B. Vasconcelos, E. Meyer, F. A. M. Sales, I. S. Moreira, L. A. Basso, and D. S. Santos, "The mode of inhibition of *Mycobacterium tuberculosis* wild-type and isoniazid-resistant 2-*trans*-enoyl-ACP(CoA) reductase enzymes by an inorganic complex," *Anti-Infective Agents in Medicinal Chemistry*, vol. 7, no. 1, pp. 50–62, 2008.

[53] J. F. Morrison, "The slow-binding and slow, tight-binding inhibition of enzyme-catalysed reactions," *Trends in Biochemical Sciences*, vol. 7, no. 3, pp. 102–105, 1982.

[54] J. V. Schloss, "Significance of slow-binding enzyme inhibition and its relationship to reaction-intermediate analogues," *Accounts of Chemical Research*, vol. 21, no. 9, pp. 348–353, 1988.

[55] P. J. Tummino and R. A. Copeland, "Residence time of receptor —ligand complexes and its effect on biological function," *Biochemistry*, vol. 47, no. 20, pp. 5481–5492, 2008.

[56] L. A. Basso, C. Z. Schneider, A. J. A. B. Dos Santos et al., "An inorganic complex that inhibits *Mycobacterium tuberculosis* enoyl reductase as a prototype of a new class of chemotherapeutic agents to treat tuberculosis," *Journal of the Brazilian Chemical Society*, vol. 21, no. 7, pp. 1384–1389, 2010.